Atmos. Meas. Tech. Discuss., 3, 4497–4530, 2010
www.atmos-meas-tech-discuss.net/3/4497/2010/
doi:10.5194/amtd-3-4497-2010

Atmospheric Measurement Techniques Discussions

Matching radiative transfer models and radiosonde data from the EPS/MetOp Sodankylä campaign to IASI measurements

X. Calbet[1], **R. Kivi**[2], **S. Tjemkes**[1], **F. Montagner**[1], **and R. Stuhlmann**[1]

[1]EUMETSAT, Eumetsat-Allee 1, 64295 Darmstadt, Germany
[2]Finnish Meteorological Institute Arctic Research Centre, Tähteläntie 62, 99600 Sodankylä, Finland

Received: 23 June 2010 – Accepted: 3 September 2010 – Published: 20 October 2010

Correspondence to: X. Calbet (xavier.calbet@eumetsat.int)

Published by Copernicus Publications on behalf of the European Geosciences Union.

Abstract

Radiances observed from IASI are compared to calculated ones. Calculated radiances are obtained using several radiative transfer models (OSS, LBLRTM v11.3 and v11.6) on best estimates of the atmospheric state vectors. The atmospheric state vectors are derived from cryogenic frost point hygrometer and humidity dry bias corrected RS92 measurements flown on sondes launched 1 h and 5 min before IASI overpass time. The temperature and humidity profiles are finally obtained by interpolating or extrapolating these measurements to IASI overpass time. The IASI observed and calculated radiances match to within one sigma IASI instrument noise in the wavenumber, ν, range of $1500 \leq \nu \leq 1570$ and $1615 \leq \nu \leq 1800\,\mathrm{cm}^{-1}$.

1 Introduction

The main purpose of the space-based remote-sensing instruments, known as hyperspectral infrared sounders, is to derive high vertical resolution atmospheric parameters from high spectral resolution measurements. This technique is usually known as "retrieval". The spectral region where hyperspectral infrared sounders usually work is from 600 to 2800 cm^{-1} and its spectral resolution is typically about 0.5 cm^{-1}. The typical noise per channel of these instruments is roughly in the range from 0.1 to 0.8 K as noise equivalent delta temperature at 280 K. Retrievals obtained with measurements made with this type of instrument achieves an accuracy of 1 K in 1 km layers for temperature profiles and between 10 to 20% relative humidity in 2 km thick layers for moisture profiles in the troposphere. Throughout this paper we will use measurements from the IASI hyperspectral infrared sounder (see Sect. 2).

Retrieval techniques usually rely on an atmospheric Radiative Transfer Model (RTM). These models try to numerically reproduce the radiation at the top of the atmosphere calculated from a given atmospheric state and surface properties. Calculated radiances are then matched to the observed ones during the retrieval process. This is

AMTD
3, 4497–4530, 2010

generally done in two different ways, statistically or with optimal estimation. Statistical methods generate a training dataset by calculating, from a representative sample of atmospheric states and RTMs, radiances at the top of the atmosphere. This dataset is used to fit a linear regression (Huang and Antonelli, 2001; Zhou et al., 2002) or other nonlinear methods like artificial neural networks (Blackwell, 2005), which are later used in an inverse way to generate the retrievals. Optimal estimation (OE) performs the retrievals by minimizing the difference between the calculated and the observed radiances and a regularisation term by using a minimizing iterative numerical method (Rodgers, 2000).

It is usually the case that RTMs cannot be used in practice as is in the retrieval schemes. They usually need to be adjusted to real world measurements. This is normally done by bias correcting the radiances and estimating the global measurement error by comparing the observed and calculated radiances for a given set of well-defined atmospheric states and surface properties (e.g., Calbet, 2006). Thus, the characterisation of the RTM with calibration measurements is a necessary and critical previous step before performing proper retrievals.

Another possible application of the comparison of hyperspectral measurements and calculated radiances using known atmospheric states and an RTM is to improve the latter by adjusting its parameters to the said observations. In order to do this, we need to be absolutely certain that we have a very precise atmospheric state vector and surface properties or we will need to have a sufficient number of observations to statistically reduce the noise in them (e.g., Strow et al., 2006).

In this paper, we will show how to correct the atmospheric states derived from the Atmospheric Sounding Campaign of the EUMETSAT Polar System (EPS) in Sodankylä to accurately describe the atmosphere. We later fit and characterise two radiative transfer models (LBLRTM and OSS, see Sect. 4) in the 1500 to 1800 cm^{-1} spectral region using space borne hyperspectral IASI data. This spectral region is where water vapour has its strongest absorption bands. The atmospheric layers that most greatly contribute to the top of the atmosphere radiances in this spectral region are located in

AMTD
3, 4497–4530, 2010

the mid to high troposphere and lower stratosphere. This fact makes these wavenumbers most insensitive to low level clouds and surface properties like emissivity and skin temperature. Because of this, the problem is greatly simplified by not having to provide a precise surface emissivity and by being able to use observations with the presence of low-level clouds.

In Sect. 2 the IASI instrument is briefly introduced. Section 3 explains the Sodankylä ground based campaign and its main instruments. The RTMs are introduced in Sect. 4. Section 5 explains how the sonde measurements are bias corrected and interpolated to reproduce the observed radiances using the RTMs. In Sect. 6 it is discussed how these measurements could be used to estimate the bias corrections and measurement error covariance matrix to be used in the retrieval techniques. Finally, conclusions are detailed in Sect. 7.

2 IASI instrument

IASI (Infrared Atmospheric Sounding Interferometer; Chalon et al., 2001; Blumstein, 2004) is a hyperspectral resolution infrared sounder onboard the polar orbiting series of Metop satellites that form the EUMETSAT Polar System (EPS). Metop-A, the first of three satellites of the series was launched successfully on 19 October 2006, from the Baikonur Cosmodrome in Kazakhstan. IASI is a Michelson interferometer measuring between 3.62 and 15.5 microns with a spectral resolution of 0.5 cm^{-1} after apodisation. The spatial resolution is 12 km at nadir.

3 IASI Sodankylä campaign and instruments

The Atmospheric Sounding Campaign of the EUMETSAT Polar System (EPS) in Sodankylä, northern Finland (location: 67.368° N, 26.633° E, 179 m asl) took place during the time period 4 June–5 September 2007. During the campaign, a total of 360 RS92

AMTD
3, 4497–4530, 2010

radiosondes, 40 ECC ozonesondes and 7 cryogenic frost-point hygrometers (CFH) were flown. The 360 radiosondes corresponded to Metop-A overpasses on each calendar day, assuming 2 soundings per each overpass during three months of operation. Ozonesondes were launched 3 times per week, CFH sondes in average two times per month. Each CFH sonde payload included also an ozonesonde and one or more RS92s. The measurements were made with the purpose to provide validation data for temperature, humidity and ozone parameters at given levels for the EPS products at the location of the campaign site. It is interesting to note that these sondes were launched specifically for calibration and validation of EPS/Metop data and its measurements have not been assimilated into any numerical weather prediction model, and particularly they have not been involved in any ECMWF analysis.

During each selected MetOp overpass, the first radiosonde launch took place 1 h and the second radiosonde launch was 5 min before the satellite overpass time. We performed, in total, four launches each day, the first two during the morning overpass and the second two during the evening overpass. In addition, regular radiosondes were launched at 23:30 and 11:30 UT each day. The ozonesondes and the CFH sondes, together with RS92 sondes, were launched during the morning overpass with the first balloon, which occurred 1 h before the satellite overpass time. During the balloon launches, continuous measurements of the temperature and water vapour profiles were obtained by a ground-based microwave radiometer and cloud base was measured by a ceilometer. In this paper, only the CFH and RS92 balloon-borne measurements have been used. It is important to note that all balloon flight measurements used in this paper were made during daytime, which, as we will see later, produces a large dry bias in the RS92 sondes.

3.1 Cryogenic frost-point hygrometer (CFH)

In Sodankylä, first flights of the CFH instrument were made in February 2004 (Suortti et al., 2008). Also several CFH comparison flights with the Fluorescent Lyman-alpha Stratospheric Hygrometer for Balloons (FLASH-B) were performed since 2005

AMTD
3, 4497–4530, 2010

confirming a good agreement with the FLASH hygrometer observations. In summer 2007, during the EPS campaign an updated version of the CFH instrument was flown in Sodankylä.

The CFH instrument was used as a reference for humidity profile measurements during our EPS campaign. The instrument measures the temperature of a mirror, which maintains a small and constant layer of frost coverage. The frost layer is kept in equilibrium with water vapour in the air passing through the sensor. Thus, the ambient frost-point is equal to the mirror temperature. The cryogenic cooling of the frost-point mirror ensures that the frost-point temperatures are achieved even in the coldest and driest layers. Relative humidity and mixing ratio can be calculated based on the frost-point temperature measurement. The design of the instrument is based loosely on the earlier versions of the frost-point mirror hygrometers by Mastenbrook and Dinger (1960) and Oltmans and Hormann (1995). Compared to its predecessors, the CFH has a more modern electronic system with a microprocessor control which has led to a simpler operation and improved reliability (Vömel et al., 2007a). Measurement uncertainty of the CFH instrument in the polar region (Sodankylä) ranges between 9% in the lower stratosphere and about 4% in the lower troposphere. The uncertainty calculation is based on the estimate of the uncertainty in frost-point temperature measurements. Several factors contribute to the uncertainty estimate leading to a total uncertainty estimate of 0.5 K in frost-point measurement, which can be considered as the upper limit of the uncertainty estimate. For later use, these figures are converted into errors in absolute relative humidity, ΔRH, which are between 0.5 and 5% in the troposphere and between 0.5 and 0.02% in the stratosphere.

3.2 RS92 radiosondes

During the EPS campaign 360 Vaisala RS92 radiosondes were flown. RS92 radiosondes have a contrasted quality as shown in its participation in the WMO radiosonde inter comparison campaign at Mauritius in 2005 (Nash et al., 2006) and in a number of other field campaigns (Suortti et al., 2008; Vömel et al., 2007b,c; Miloshevich et al., 2009).

AMTD
3, 4497–4530, 2010

The RS92 sonde has been manufactured since 2004 and the changes to the sensor have been documented by Vaisala (2010).

The temperature measurements of these sondes are made by a capacitive wire type of sensor which has a response time better than 1 s below 100 hPa. Temperature accuracy is ±0.2 °C at the 2-sigma level throughout the troposphere for nighttime measurements (Paukkunen et al., 2001).

The RS92 humidity sensor is a thin film capacitor that directly measures relative humidity. It consists of two sensors, which are alternately measuring and being heated, thus, eliminating coating of the sensor by ice or liquid inside clouds. Miloshevich et al. (2006) tested a number of operational radiosondes. They found that RS92 humidity was the most accurate among the tested sondes. They suggested corrections to the standard humidity product, after which the RS92 mean accuracy relative to the reference instrument was found to be better than 1% in the lower troposphere, < 2% in the middle troposphere and < 3% in the upper troposphere. These relative errors translate into absolute errors in relative humidity, ΔRH, between 0.2 and 3%.

Although this accuracy seems to be within bounds, unfortunately the previous versions of the RS92 instruments, which were not used in this campaign, suffer from a very large radiation dry bias (Vömel et al., 2007b) when used during daytime which can range from 9 to 50% in absolute terms of relative humidity (ΔRH). One of the important improvements to the latest version is the new coating of humidity sensor contacts in late 2006 Vaisala (2010). These improved sondes (360 sondes altogether) were the ones flown during our campaign in summer 2007. The new coating method was intended to reduce the radiation dry bias found earlier during the RS92 sonde daytime measurements (Vömel et al., 2007b). To confirm this dry bias and to see differences between the two RS92 versions, we made a series of seven RS92/CFH comparison flights during the EPS/Metop campaign in summer 2007. In each payload, we had the new and the old version of the RS92 sonde and the CFH instrument as a reference (Kivi et al., 2009). We found that the new method reduces the radiation dry bias at the altitude of 300 hPa by about 5%, but does not completely remove the daytime dry bias.

AMTD
3, 4497–4530, 2010

Therefore, we derived an empirical correction method, which is similar to the Vömel et al. (2007b) method, but it corresponds to the newer sonde types that we used during the EPS campaign (Fig. 1). For the type of RS92 sondes used during the EPS campaign the radiation bias correction can be calculated by (Kivi et al., 2009):

$$C_{\mathrm{rad}}(p) = -0.01376\ln(p)^2 + 0.3018\ln(p) - 0.445, \quad (1)$$

where p is pressure in hectopascals. The corrected relative humidity, $\mathrm{RH}_{\mathrm{corr}}$, values can be derived as

$$\mathrm{RH}_{\mathrm{corr}} = \mathrm{RH}/C_{\mathrm{rad}}, \quad (2)$$

where RH is the uncorrected relative humidity measured by the RS92 humidity sensor.

4 Radiative transfer models

We will make the comparison using three different radiative models:

- OSS trained with LBLRTM 11.3
- LBLRTM version 11.3
- LBLRTM version 11.6

These three models are described in more detail below.

4.1 LBLRTM

Accurate spectra at the top of the atmosphere were generated using the Line By Line Radiative Transfer Model (LBLRTM, Clough et al., 2005). LBLRTM has a long development history and for the current study version 11.6 was adopted together with spectroscopical parameters from the HITRAN 2004 database including updates. LBLRTM is

AMTD
3, 4497–4530, 2010

a versatile high accurate radiation code which describes the interaction between matter and radiation at a single wavenumber. The accuracy of LBLRTM was documented in several publications (e.g., Tjemkes et al., 2003). For comparison with the results generated by OSS as described below, radiances at the top of the atmosphere with LBLRTM v11.3 and AER V2.1 were also generated. Differences between the two versions include modifications in the water vapour continuum, besides some bug fixing problems. Most important changes were related to the line coupling description, which avoided the calculation of the so-called chi-factor.

4.2 OSS

As detailed line-by-line calculations are time consuming, a fast radiative transfer code was used as well to understand how this fast code can capture the radiances at the top of the atmosphere. The particular fast radiative transfer code adopted here was the so-called Optimal Spectral Sampling (OSS) radiative transfer model described by Moncet at al. (2008). The OSS code solves the radiative transfer equation at a single wavenumber similar to the LBLRTM code. Contrary to LBLRTM, the OSS code uses only a small set of discrete wavenumbers. The accuracy of OSS depends on the adopted discrete set. The set of wavenumbers is specific for each space-borne instrument and are derived from an elaborate training process. The training data employs results by LBLRTM for a representative set of atmospheric state. This database was generated using version 11.3 of LBLRTM with the AER V2.1 of the HITRAN line database.

5 Comparison of observed and calculated radiances

5.1 Scenes

The IASI radiances used in this study where measured over Sodankylä and where co-located in time with the CFH sondes from the EPS/Metop campaign. The exact dates

AMTD
3, 4497–4530, 2010

and times are shown in Table 1. The AVHRR images corresponding to these scenes were analysed visually to check for clouds. All of the scenes had a higher or smaller degree of underlying low level clouds. Two of the scenes contained high level cirrus and could not be used in the comparison. For one scene there was no IASI data available in the archive. This leaves a final result of four scenes where we can intercompare IASI observations. See Table 1 for particular details.

5.2 Sonde measurements

Let us recall here that we will use in this paper one RS92 and one CFH sonde launched 1 h before overpass time and an RS92 sonde launched 5 min before overpass time. To have a sense of how much the sondes have drifted away from the launch location, we plot Fig. 2. In this figure, we show the trajectories of the CFH sondes of the four selected scenes from Table 1.

For illustration purposes, the time and vertical scales are plotted in Fig. 3. In this figure, we can see the ascent and descent for one particular day of the CFH sonde launched 1 h before overpass time and the ascent of the RS92 sonde launched 5 min before overpass time. The overpass time is plotted as a vertical line. This figure gives an idea of the vertical position of the sondes relative to the overpass time. It also constitutes a picture of the time interpolation that needs to be done to fit the observed radiances to the calculated ones.

Radiosonde measurements for two particular days are shown in Figs. 4 and 5. We can see the profile for the CFH and RS92 sonde launched 1 h before overpass time (red and green, respectively), the RS92 sonde launched 5 min before IASI overpass (in black) and the ECMWF analysis profile approximately 3 h after (in blue) and 3 h before satellite overpass in blue (in gray). These figures show several interesting features of the sonde measurements:

– Temperature profiles from all sondes and ECMWF analyses tend to agree pretty well between each other.

AMTD
3, 4497–4530, 2010

– Moisture from RS92 profiles are not usable above the tropopause level, usually between 200 to 300 hPa. Whenever we calculate radiances for this type of profile, we substitute the moisture above this level with the CFH sonde measurements.

– Moisture measured with the CFH sonde does not seem to measure properly above approximately 40 hPa. Whenever we calculate radiances for this type of profile, we substitute the moisture above this level with the ECMWF analyses.

– Moisture profiles can vary substantially between sondes launched 1 h and 5 min before overpass. We can see this in Fig. 4 at the 400 hPa level.

– Upper troposphere, lower stratosphere moisture from ECMWF analyses can be substantially different to the ones measured with the CFH or RS92 sonde (see Fig. 5 at 200 hPa).

5.3 Sonde corrections

Observed radiances measured with IASI should be compared with calculated radiances using the best known atmospheric state vectors available and the LBLRTM (11.3 and 11.6) or OSS RTMs. CFH sondes are always taken as a reference, assuming that they measure perfectly in all conditions and no corrections are applied to them (except above 40 hPa, where we insert ECMWF analyses, as we have seen). On the other hand, RS92s show a large dry bias in the humidity measurements when measuring during daytime, which we have to correct for. This dry bias is believed to be caused by solar radiation impinging on the detectors (Vömel et al., 2007b). It is important to note that because of this, it is difficult to model and precisely correct individually each radiosonde measurement. Three different types of humidity corrections have been applied to the RS92s in this paper:

– What we will call "in situ" bias corrections, which consists of calibrating each day independently by calculating the dew point temperature difference between the CFH sonde and the RS92 measurement flown on the same balloon, which were

AMTD
3, 4497–4530, 2010

launched 1 h before IASI overpass time. This bias correction is then applied to restore the RS92 sonde measurement launched 5 min before satellite overpass time. Since the radiation conditions within 1 h between both radiosonde observations during the Sodankylä summer morning should not change much, this method should account for the fine detail of the dry bias as the balloon ascends in the atmosphere and its incident radiation conditions change.

– In general, a correction, which depends on pressure, is available that works statistically on average (Vömel et al., 2007b). As we have seen (Eqs. 1 and 2), in this paper we will use a slightly modified version of this bias correction targeted specifically to the modified RS92 radiosondes used here (Kivi et al., 2009). These bias corrections should be re-calculated (Kivi et al., 2009) every time a new modification of RS92 sondes is used. We will denominate this as "Kivi et al." bias correction. It is important to note that the coefficients for this bias correction (Eq. 1) have been obtained from the comparison of CFH and RS92 sondes flying with the same balloons launched 1 h before satellite overpass time combining all days together, but have been applied to the RS92s sondes launched 5 min before IASI overpass time of those very same days. In other words, although the corrections are a statistical combination of measurements from several different days, they are applied to those same days which most probably have very similar solar radiation conditions. It remains to be proven whether this kind of corrections can be applied between two completely different sets of measurements or solar radiation conditions.

– For illustration purposes, and because it fits better with the OSS model, we will use a third bias correction which is the "Kivi et al." one corrected with a 2% additional relative humidity, which we will denote as "Kivi et al. +2",

$$RH_{corr} = RH/C_{rad} + 2. \quad (3)$$

AMTD
3, 4497–4530, 2010

To illustrate this procedure, we have plotted the observed minus calculated radiance differences after each one of the corrections proposed here are applied to the data. To begin with, we plot the observed minus calculated radiances obtained with the raw radiosonde data and the OSS RTM for a particular sample day in Fig. 6. In blue we plot the difference for the CFH sonde which was launched 1 h before IASI overpass time. In green is the difference for the RS92 sonde launched 5 min before satellite overpass. Thin, black, nearly flat lines correspond to three sigma IASI instrument noise, or more specifically to three times the diagonal of the IASI covariance matrix instrument noise provided by CNES (explained in detail in Pequignot et al., 2008). As we can see, the calculated radiances are significantly off the plus minus three sigma IASI instrument noise band.

We now correct the RS92 sonde measurements with the three different dry bias corrections. The observed minus calculated radiances using the "in situ" moisture correction are shown in Fig. 6 as a red line. In Fig. 7 the observed minus calculated radiances using the Kivi et al. moisture correction are shown in Fig. 7 again as a red line. Finally, in Fig. 8 the difference using the "Kivi et al. +2" bias correction is shown also in red. We see the big improvement the RS92 measurements have undergone for all bias corrections, lying now within the plus minus three sigma IASI instrument noise band.

The next step is to co-locate in space and time the IASI measurement with the radiosonde observations, which will always inevitably never coincide with the satellite overpass.

Regarding spatial co-location, the radiosonde locations are plotted in Fig. 2. This figure shows that the radiosondes do not drift very far away from the launch location. For this reason, together with the fact that we are studying IASI channels which have contributions of temperature and moisture from the mid-troposphere to the low stratosphere, which usually show small spatial variability, we have not attempted any spatial co-location corrections. We are, thus, effectively assuming that all radiosondes are perfectly spatially co-located with the IASI fields of view. The validity of this assumption

AMTD
3, 4497–4530, 2010

will rely on the results obtained.

Time co-location is achieved by combining the CFH sondes launched 1 h before overpass time and the bias corrected humidity ones (RS92) launched 5 min before satellite overpass. A linear interpolation or extrapolation to the overpass time per altitude level (see Fig. 3) is done with these sonde temperature and moisture profiles in a similar fashion to Tobin et al. (2006). Results of the observed minus calculated radiances for the interpolated profiles are shown as a black line in Figs. 6–8 with the three different bias corrections. With these final interpolated profiles, radiances improve significantly and are fitted within three sigma IASI instrument noise band.

We can now summarize the results of all these measurements by normalizing the radiance residuals with the IASI instrument noise and plotting a histogram of them. For this, we select wavenumbers, ν, not affected by clouds, $1500\,\mathrm{cm}^{-1} \leq \nu \leq 1570\,\mathrm{cm}^{-1}$ and $1615\,\mathrm{cm}^{-1} \leq \nu \leq 1800\,\mathrm{cm}^{-1}$. The results generated by interpolating the temperature and water vapour sondes with the "in situ" and the Kivi et al. bias corrections for the three different RTMs OSS, LBLRTM 11.3 and LBLRTM 11.6 are shown in Figs. 9–11, respectively. A one sigma Gaussian curve is plotted on top of the histograms as a dotted line for comparison purposes. We can see that all models and all bias corrections fit very well with a one sigma Gaussian function. The only difference is the slight displacement of one Gaussian figure with respect to the others. OSS seems to fit better with the "in situ" bias correction, while LBLRTM 11.6 seems to fir better with the Kivi et al. bias correction. To understand the origin of this slight displacement or bias of these curves we have plotted Fig. 12. It shows the "in situ" and the Kivi et al. +2 dry bias corrections together with the OSS RTM. In this case, all three Gaussian curves overlap. This shows that the difference between all the plotted Gaussian figures is a mere 2% bias correction in the absolute relative humidity. Which means IASI is sensitive enough to see the presence of this small bias difference throughout the whole atmospheric profile. Clearly, the instrumentation available, as well as the knowledge in the RTMs does not allow us to infer which of the positions of the Gaussian curves, or biases, is the correct one.

AMTD
3, 4497–4530, 2010

In Fig. 13 we plot the histograms separately for each of the four observation days. We can verify how the histograms of all four days fit well to a one sigma Gaussian distribution.

6 Retrieval bias corrections and measurement error covariance matrix

The bias corrections and the measurement error covariance matrix which would optimize our retrievals (Calbet, 2006) would be the mean and standard deviation (ideally, it should be the full covariance matrix) of the observed minus calculated radiances shown above. Unfortunately, we only have four cases from which it is difficult to draw a representative statistics. Nevertheless, for illustration purposes, we plot the mean and standard deviation of such differences in Fig. 14 only for the OSS and "in situ" bias correction. We can see how the bias is mostly contained within the one sigma IASI instrument noise and the standard deviation fluctuates around this value.

7 Conclusions

We have proved that, with adequate radiosonde measurements and RTM, it is possible to reproduce IASI measurements to within the accuracy of one sigma instrument noise. The measurement methodology that has been proven useful is based on launching a CFH and an RS92 sondes 1 h and an RS92 sonde 5 min before satellite overpass time.

To reproduce these results, we need sonde measurements with an extremely low bias $< 0.2\%$ in absolute terms and high accuracy of relative humidity, especially in the upper troposphere and low stratosphere (where RS92 and ECMWF analysis are not reliable). The only sonde instruments that can get close to these numbers seem to be the CFH sondes.

We have seen that IASI radiances are sensitive to a very low bias difference of only 2% in absolute relative humidity. Although IASI is not sensitive enough to detect such

AMTD
3, 4497–4530, 2010

small differences in one single layer, it is sensitive enough to detect this small bias applied to the whole humidity profile. Because this range of humidities is within the limits of the measuring devices used in this paper and also within the accuracies of the present RTMs, we can only say that the RTMs are in agreement with the observations, from the bias point of view, to within about 2% (ΔRH).

Spatial co-location does not seem to play a big role in the radiance matching, but temporal co-location and time interpolation seems to be critical in achieving these results.

The question that immediately arises is whether we can achieve these same results using RS92 sondes only, which would be beneficial because of the savings involved. The answer is not clear. It would appear to have a positive answer because we are also achieving good results with a statistical correction Kivi et al. (2009). But we have to remember that this correction has been calculated with the comparison of CFH and RS92 sondes from this same campaign, resulting in a slightly incestuous process. The radiance match would clearly not work using the more standard Vömel et al. (2007b) RS92 corrections, recalling that the RS92 humidity sensors used here are significantly different from the ones in Vömel et al. (2007b). A humidity bias correction calculated and applied at the same day in similar observing conditions (what we have called "in situ" correction) seems to be the more physical way to proceed, but at the cost of having to launch a CFH sonde. To summarize, it is difficult to asses whether these same results could be achieved with RS92 sondes only, but the fact that we had to use bias corrections calculated in similar observing conditions as the measurements which needed to be corrected seems to imply that CFH (or similar) quality measurements are necessary. On the other hand, from the comparisons of RS92s, CFHs and ECWMF analysis we know that the only method that will give a reliable measurement of humidity in the upper troposphere/low stratosphere are the CFHs (see Fig. 5 and Sect. 5.2).

If we want to have significant statistics to derive proper bias corrections and measurement error covariance matrices for retrieval purposes and possibly further advance the RTMs with these kind of data comparisons we will need far more data than the

AMTD
3, 4497–4530, 2010

one provided from this campaign. It would be advisable, if possible, to extend these kind of measurements by taking advantage of the current or planned networks of high accuracy atmospheric state characterisation (GRUAN, 2010) by co-location in time these measurements with hyperspectral sensor overpasses. This would increase the matches by a significant amount at an affordable cost due to the synergy. On the other hand, it is expected to have in the future hyperspectral infrared sounders in geostationary orbit providing measurements in roughly 1 h time intervals which should be simple enough to co-locate with existing high measurement accuracy networks.

Acknowledgements. Almost all figures and calculations in this document have been made using the free software numerical analysis package called PDL (http://pdl.perl.org).

References

Blackwell, W. J.: A neural-network technique for the retrieval of atmospheric temperature and moisture profiles from high spectral resolution sounding data, IEEE T. Geosci. Remote, 43, 2535–2546, 2005. 4499

Blumstein, D., Chalon, G., Carlier, T., Buil, C., Hébert, P., Maciaszek, T., Ponce, G., Phulpin, T., Tournier, B., and Siméoni, D.: IASI instrument technical overview and measured performances, SPIE Conference, Denver (Co), SPIE 2004-5543-22, August 2004. 4500

Calbet, X. and Schlüssel, P.: Technical note: analytical estimation of the optimal parameters for the EOF retrievals of the IASI Level 2 Product Processing Facility and its application using AIRS and ECMWF data, Atmos. Chem. Phys., 6, 831–846, doi:10.5194/acp-6-831-2006, 2006. 4499, 4511

Chalon, G., Cayla, F., and Diebel, D.: IASI: An Advanced Sounder for Operational Meteorology, Proceedings of the 52nd Congress of IAF, Toulouse France, 1–5 Oct., 2001. 4500

Clough, S. A., Shephard, M. W., Mlawer, E. J., Delamere, J. S., Iacono, M. J., Cady-Pereira, K., Boukabara, S., and Brown, R. D.: Atmospheric radiative transfer modeling: a summary of the AER codes., J. Quant. Spectrosc. Ra., 91, 233–244, 2005. 4504

GRUAN: Weather and Climate – Deutsche Wetterdienst – Startseite GRUAN, http://www.dwd.de/gruan, last access: 18 October, 2010.

AMTD
3, 4497–4530, 2010

Huang, H. and Antonelli, P.: Application of principal component analysis to high-resolution infrared measurement compression and retrieval, J. Appl. Meteorol., 40, 365–388, 2001. 4499

Kivi, R., Kujanpää, J., Aulamo, O., Heikkinen, P., Hassinen, S., Calbet, X., Montagner, F., and Vömel, H.: Observations of water vapor profiles over Northern Finland by satellite and balloon borne instruments, in: Proceedings: 2009 EUMETSAT Meteorological Satellite Conference, 21–25 September 2009, Bath, UK, EUMETSAT P.55, 2009. 4503, 4504, 4508, 4512

Mastenbrook, H. J. and Dinger, J. E.: The measurement of water vapor distribution in the stratosphere, Tech. Rep. NRL 5551, 35 pp., Nav. Res. Lab., Washington D. C., 1960. 4502

Miloshevich L. M., Vömel, H., Whiteman, D. N., Lesht, B. M., Schmidlin, F. J., and Russo, F.: Absolute accuracy of water vapor measurements from six operational radiosonde types launched during AWEX-G and implications for AIRS validation, J. Geophys. Res., 111, D09S10, doi:10.1029/2005JD006083, 2006. 4503

Miloshevich, L. M., Vömel, H., Whiteman, D. N., and Leblanc, T.: Accuracy assessment and correction of Vaisala RS92 radiosonde water vapor measurements, J. Geophys. Res., 114, D11305, doi:10.1029/2008JD011565, 2009. 4502

Nash, J., Smout, R., Oakley, T., et al.: WMO Intercomparison of High Quality Radiosonde Systems, Vacoas, Mauritius, 2–25 February 2005, Instruments and observing methods report No. 83, WMO, Geneva, Switzerland, 2006. 4502

Moncet, J., Uymin, G., Lipton, A. E., and Snell, H. E.: Infrared radiance modeling by optimal spectral sampling, J. Atmos. Sci., 65, 3917–3934, 2008. 4505

Oltmans, S. J. and Hofmann, D. J.: Increase in lower-stratospheric water vapour at a midlatitude Northern Hemisphere site from 1981 to 1994, Nature, 374, 146–149, 1995. 4502

Paukkunen, A., Antikainen, V., and Jauhiainen, H.: Accuracy and performance of the new Vaisala RS90 radiosonde in operational use, paper presented at 11th Symposium on Meteorological Observations and Instrumentation, Am. Meteorol. Soc., Albuquerque, N. M., 14–18, Jan, 2001. 4503

Pequignot, E., Blumstein D., and Larigauderie, C.: CNES Technical Note: IASI Noise Covariance Matrix, IA-TN-0000-3271-CNE, 2008. 4509

Rodgers, C. D.: Inverse methods for atmospheric sounding. Theory and practice, World Scientific, Singapore, 2000. 4499

Strow, L. L., Hannon, S. E., De-Souza Machado, S., Motteler, H. E., and Tobin, D. C.: Validation of the Atmospheric Infrared Sounder radiative transfer algorithm, J. Geophys. Res., 111,

AMTD
3, 4497–4530, 2010

D09S06, 2006. 4499
Suortti, T. M., Kats, A., Kivi, R., Kämpfer, N., Leiterer, U., Miloshevich, L. M., Neuber, R., Paukkunen, A., Ruppert, P., Vömel, H., and Yushkov, V.: Tropospheric comparisons of Vaisala radiosondes and balloon-borne frost-point and Lyman-α hygrometers during the LAUTLOS-WAVVAP experiment, J. Atmos. Ocean. Tech., 25, 149–166, 2008. 4501, 4502
Tjemkes, S. A., Patterson, T., Rizzi, R., Shephard, M. W., Clough, S. A., Matricardi, M., Haigh, J. D., Hopfner, M., Payan, S., Trotsenko, A., Scott, N., Rayer, P., Taylor, J. P., Clerbaux, C., Strow, L. L., DeSouza-Machado, S., Tobin, D., and Knuteson, R.: The ISSWG line-by-line inter-comparison experiment, J. Quant. Spectrosc. Ra., 77, 433–453, 2003. 4505
Tobin, D. C., Revercomb, H. E., Knuteson, R. O., Lesht, B. M., Strow, L. L., Hannon, S. E., Feltz, W. F., Moy, L. A., Fetzer, E. J., Cress, T. S.: Atmospheric radiation measurement site atmospheric state best estimates for atmospheric infrared sounder temperature and water vapor retrieval validation, J. Geophys. Res., 111, D09S14, 2006. 4510
Vaisala, Data continuity (available at http://www.vaisala.com/weather/products/datacontinuity.html), 2010. 4503
Vömel, H., David, D. E., and Smith, K.: Accuracy of tropospheric and stratospheric water vapor measurements by the cryogenic frost point hygrometer: Instrumental details and observations, J. Geophys. Res., 112, D08305, doi:10.1029/2006JD007224, 2007a. 4502
Vömel, H., Selkirk, H., Miloshevich, L., Valverde-Canossa, J., Valds, J., Kyrö, E., Kivi, R., Stolz, W., Peng, G., and Diaz, J. A.: Radiation dry bias of the Vaisala RS92 humidity sensor, J. Atmos. Ocean. Tech., 24, 953–963, 2007b. 4502, 4503, 4504, 4507, 4508, 4512
Vömel, H., Yushkov, V., Khaykin, S., Korshunov, L., Kyrö, E., and Kivi, R.: Intercomparisons of stratospheric water vapor sensors: FLASH-B and NOAA/CMDL frost-point hygrometer, J. Atmos. Ocean. Tech., 24, 941–952, 2007c. 4502
Zhou, D. K., Smith, W. L., Li, J., Howell, H. B., Cantwell, G. W., Larar, A. M., Knuteson, R. O., Tobin, D. C., Revercomb, H. E., and Mango, S. A.: Thermodynamic product retrieval methodology and validation for NAST-I, Appl. Optics, 4, 6957–6967, 2002. 4499

AMTD
3, 4497–4530, 2010

Table 1. Dates and times of IASI observations over Sodankylä with co-located CFH sondes. Comments concerning cloud information have been obtained from visual inspection of AVHRR images.

Date	Time (UT)	Used in comparison with RTM	Comment
15 Jun 2007	09:20:42	Yes	Low level clouds
13 Jul 2007	09:41:20	Yes	Low level clouds
17 Jul 2007	08:18:23	Yes	FOV mostly clear with some low level clouds
20 Jul 2007	08:56:26	No	No IASI data in archive
25 Jul 2007	08:52:59	Yes	Low level clouds
2 Aug 2007	09:27:34	No	Low level clouds plus thin cirrus
22 Aug 2007	09:13:47	No	Thick cirrus

AMTD
3, 4497–4530, 2010

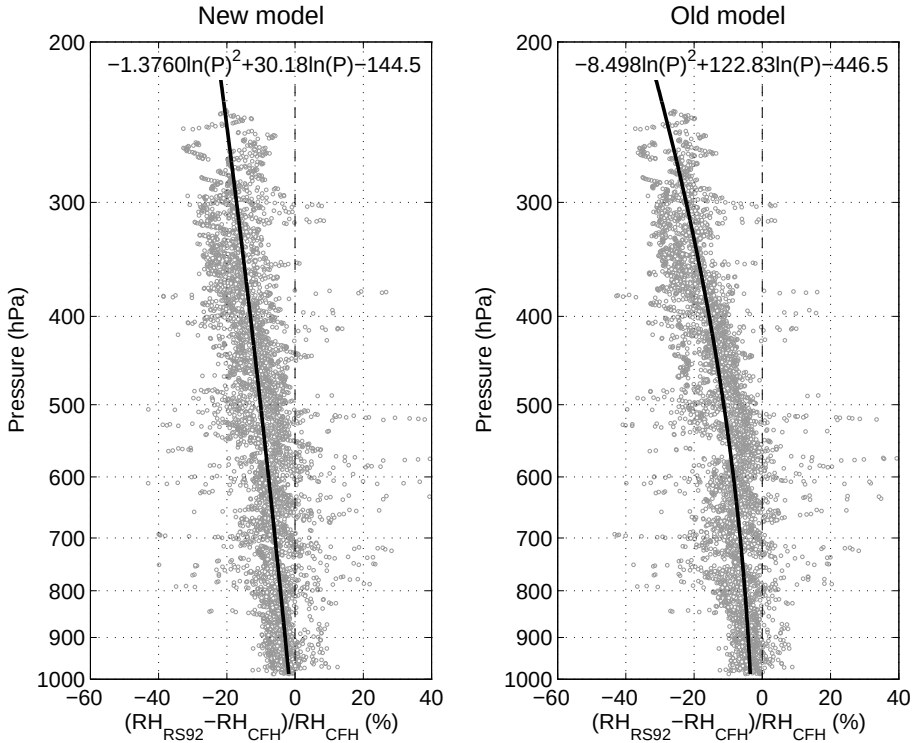

Fig. 1. Relative difference between RS92 and CFH (cryogenic frost point hygrometer) humidity profiles during daytime flights in Sodankylä from June to August 2007. The new model of the RS92 sonde (left) is using aluminized coating of the sensor attachment, which reduces the radiation dry bias compared to the earlier version of the RS92 (right). Both RS92 sonde models and also the CFH sonde were flown in the same balloon payload during the EPS/Metop Sodankylä campaign. The CFH sonde is here used as a reference for both RS92 sonde models.

AMTD
3, 4497–4530, 2010

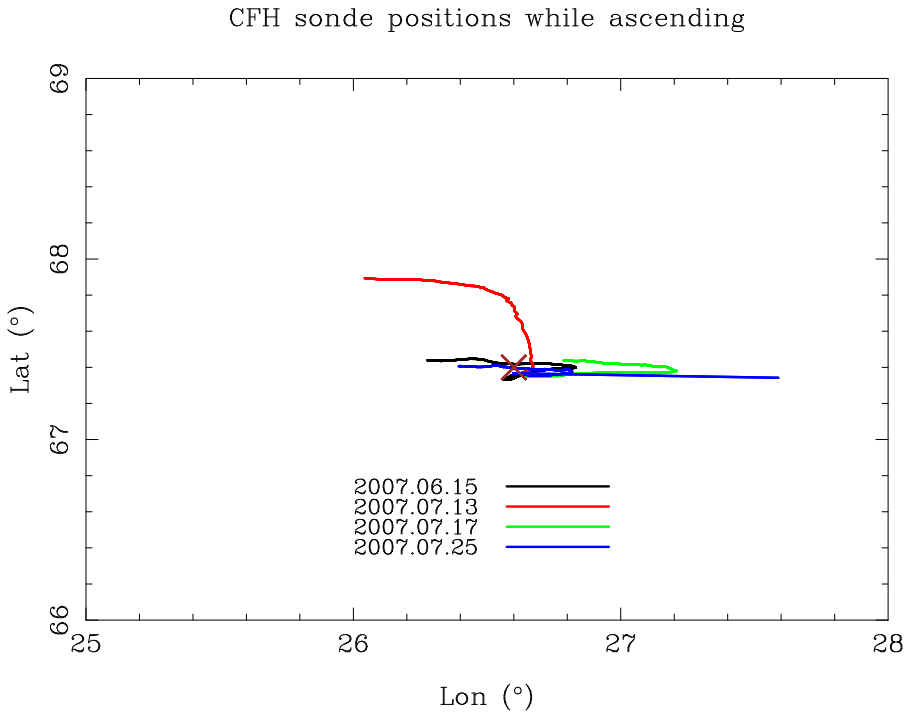

Fig. 2. Ascending trajectories of the four CFH sondes selected for comparison as shown in Table 1. The big brown cross in the centre is the launch location at the FMI Artic Research Centre observatory in Sodankylä.

AMTD
3, 4497–4530, 2010

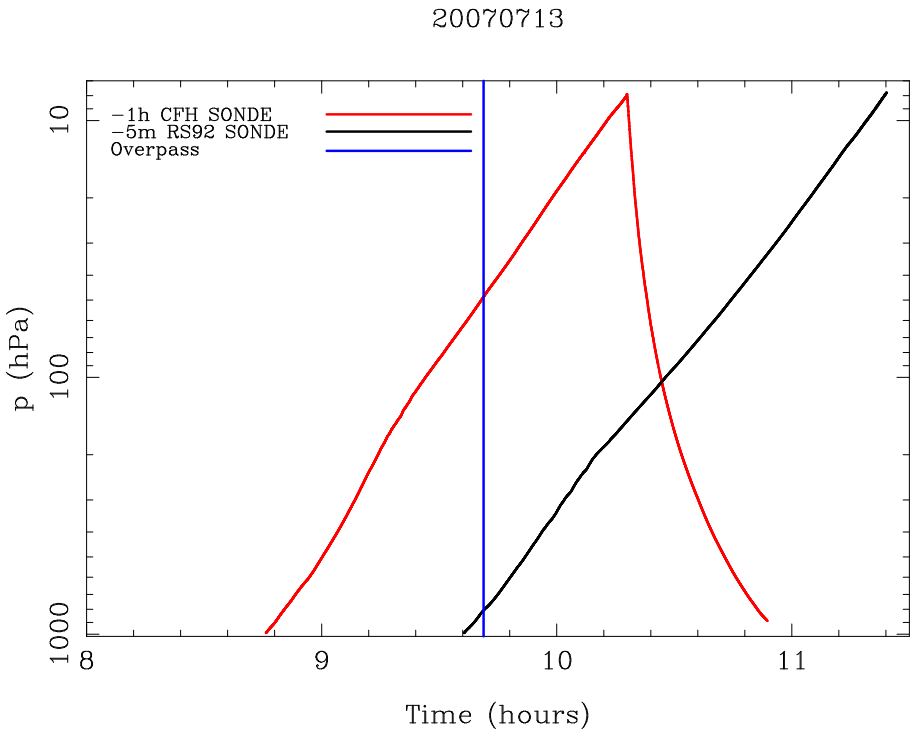

Fig. 3. Vertical position of the sonde versus time. The sonde, which carries an RS92 and a CFH, launched 1 h before overpass time is plotted (red) together with the sonde, carrying only an RS92, launched 5 min before overpass time (black). The overpass time is plotted as a vertical line (blue).

AMTD
3, 4497–4530, 2010

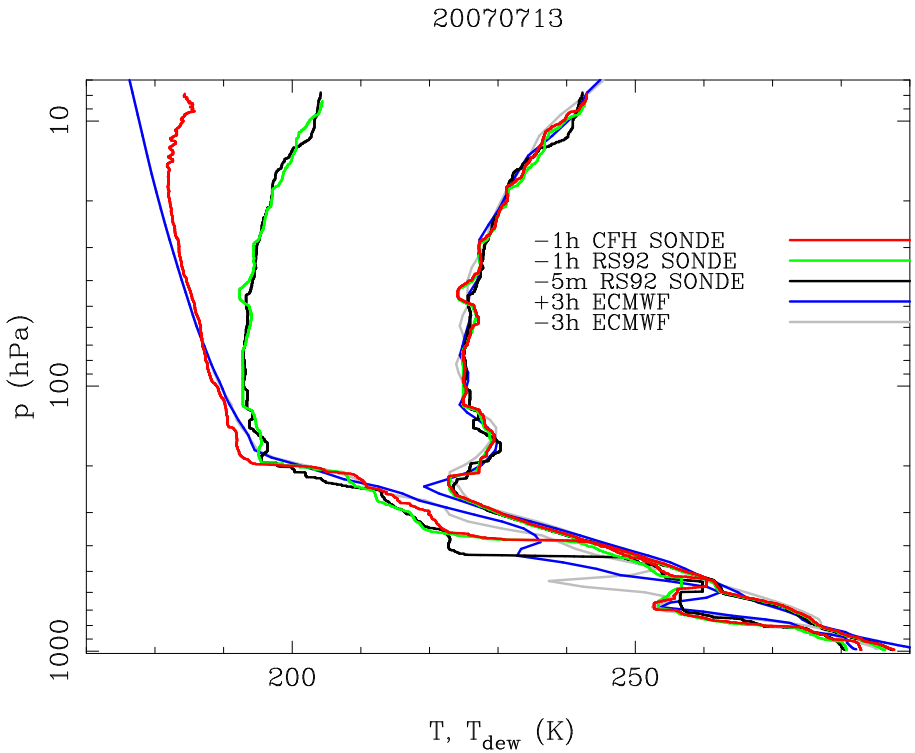

Fig. 4. Temperature (right) and water vapour profiles (left) for the CFH and RS92 sonde launched 1 h before overpass time (red and green, respectively), the RS92 sonde launched 5 min before IASI overpass (black) and the ECMWF analysis profile approximately 3 h before and after satellite overpass (gray and blue, respectively). Note the big moisture variation between the 1 h and 5 min before overpass launch measurements at the 400 hPa-level.

AMTD
3, 4497–4530, 2010

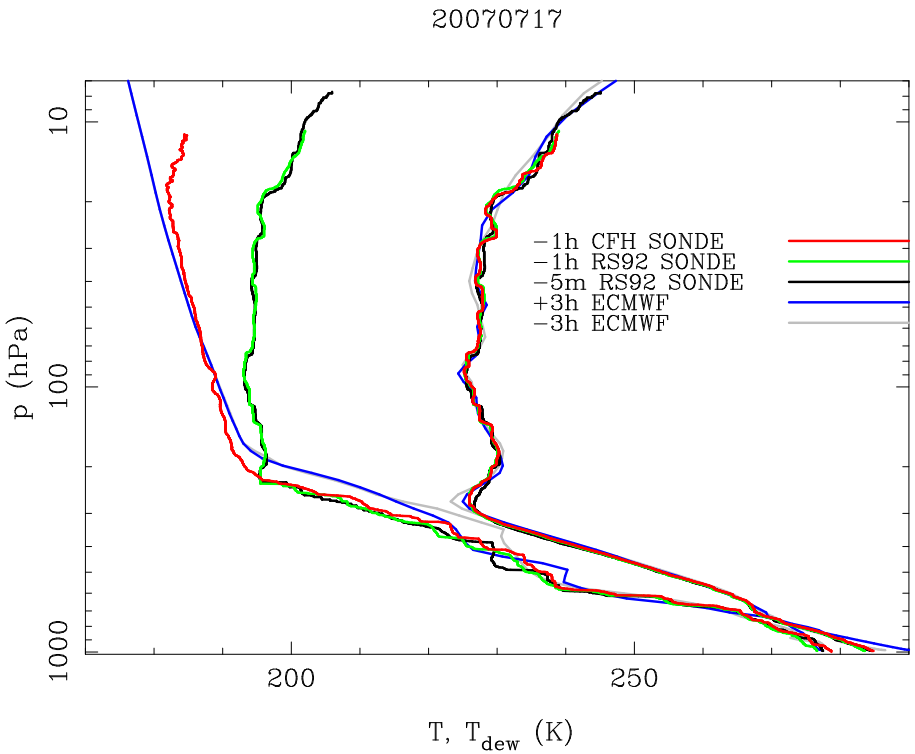

Fig. 5. Temperature (right) and water vapour profiles (left) for the CFH and RS92 sonde launched 1 h before overpass time (red and green, respectively), the RS92 sonde launched 5 min before IASI overpass (black) and the ECMWF analysis profile approximately 3 h before and after satellite overpass (gray and blue, respectively). Note the big difference between the ECMWF analyses and the radiosondes moisture at 200 hPa.

AMTD
3, 4497–4530, 2010

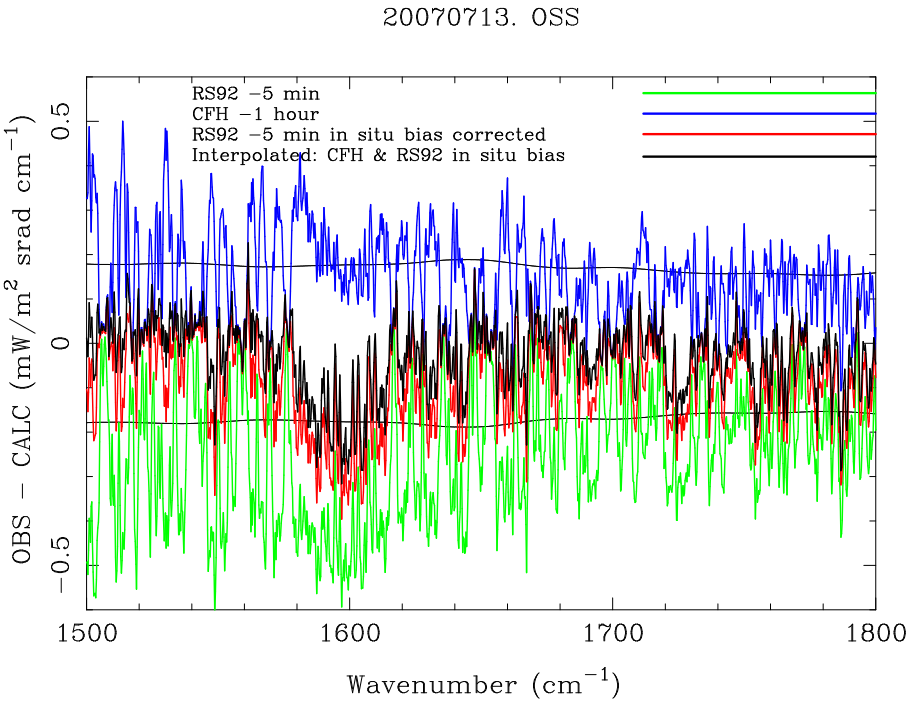

Fig. 6. Residual radiances, IASI observed minus calculated with OSS RTM, for different atmospheric profiles: CFH sonde launched 1 h before overpass (blue), RS92 sonde launched 5 min before overpass (green), same sonde but with the "in situ" bias correction (red) and the time interpolated profile (black) using CFH (launched 1 h before overpass) and "in situ" bias corrected RS92 (launched 5 min before overpass) measurements. Thin black nearly flat lines correspond to three sigma IASI instrument noise.

AMTD
3, 4497–4530, 2010

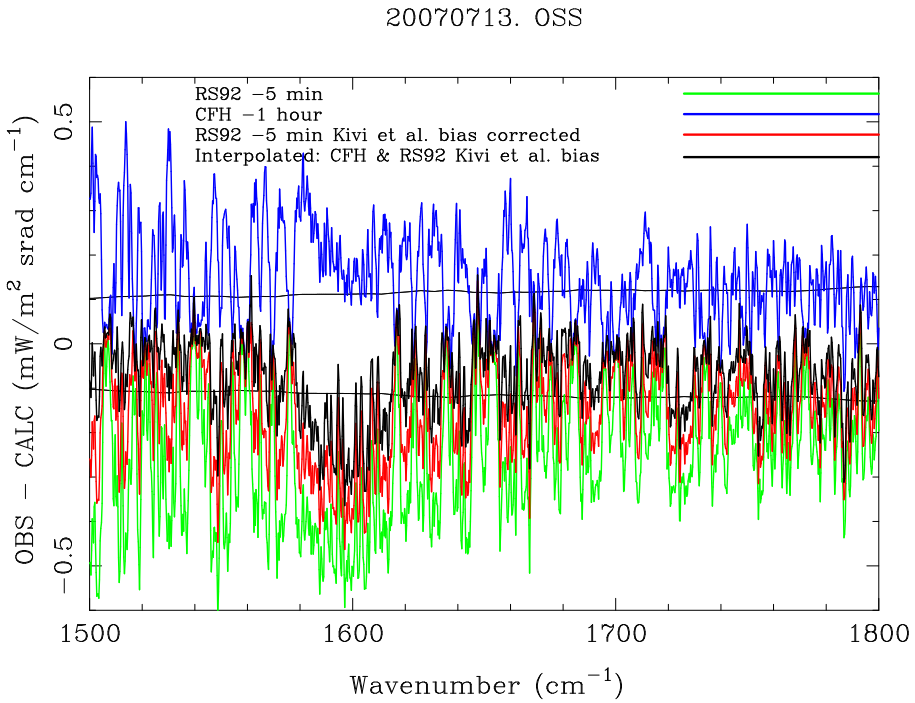

Fig. 7. Residual radiances, IASI observed minus calculated with OSS RTM, for different atmospheric profiles: CFH sonde launched 1 h before overpass (blue), RS92 sonde launched 5 min before overpass (green), same sonde but with the Kivi et al. bias correction (red) and the time interpolated profile (black) using CFH (launched 1 h before overpass) and Rigel et al. bias corrected RS92 (launched 5 min before overpass) measurements. Thin black nearly flat lines correspond to three sigma IASI instrument noise.

AMTD
3, 4497–4530, 2010

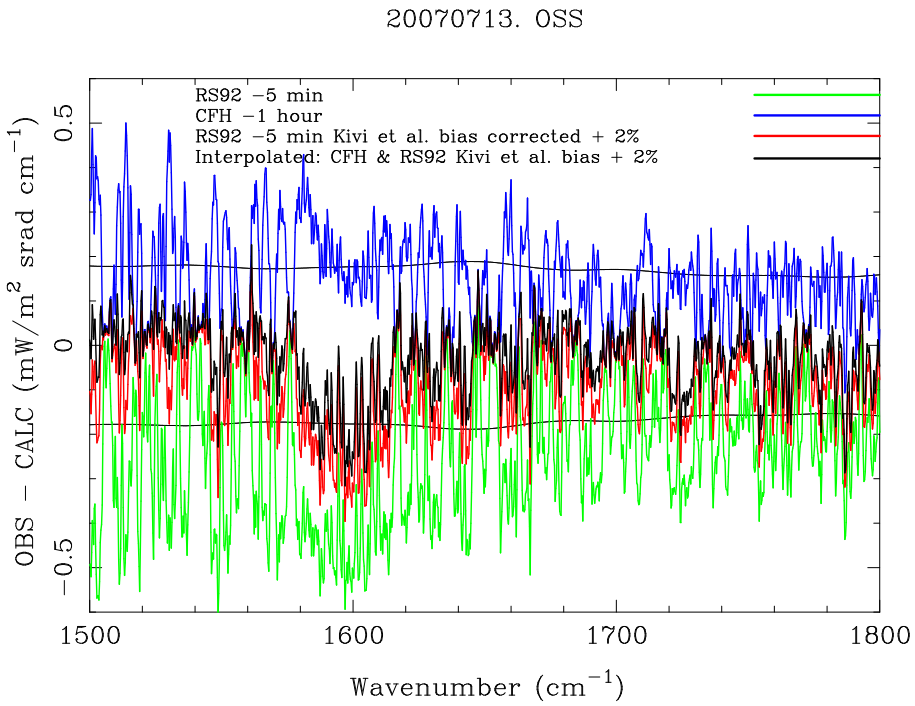

Fig. 8. Residual radiances, IASI observed minus calculated with OSS RTM, for different atmospheric profiles: CFH sonde launched 1 h before overpass (blue), RS92 sonde launched 5 min before overpass (green), same sonde but with the "Kivi et al. +2" bias correction (red) and the time interpolated profile (black) using CFH (launched 1 h before overpass) and Rigel et al. bias corrected RS92 (launched 5 min before overpass) measurements. Thin black nearly flat lines correspond to three sigma IASI instrument noise.

AMTD
3, 4497–4530, 2010

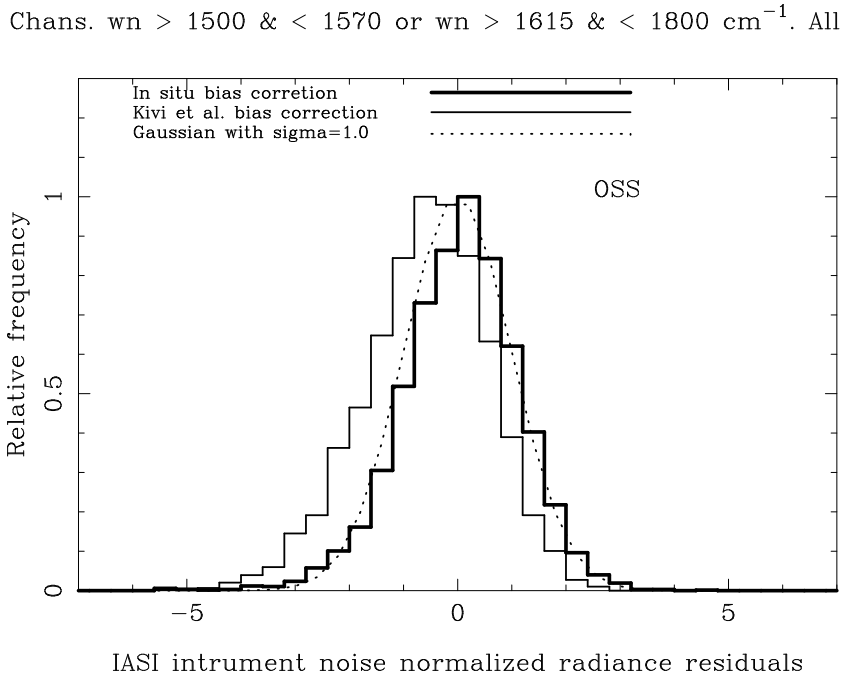

Fig. 9. Histogram of the residual radiances, IASI observed minus calculated with OSS RTM and two time interpolated profiles, for all clear days (4) in the spectral range, 1500 cm^{-1} ≤ ν ≤ 1570 cm^{-1} and 1615 cm^{-1} ≤ ν ≤ 1800 cm^{-1}. One interpolated profile has been derived from the CFH sonde launched 1 h before IASI overpass and the "in situ" bias corrected RS92 sonde launched 5 min before satellite overpass (thick solid line). The other interpolated profile has been derived from the CFH sonde launched 1 h before IASI overpass and the Kivi et al. bias corrected RS92 sonde launched 5 min before satellite overpass (thin solid line). For reference, a Gaussian curve with a σ of 1.0 is shown (dotted line).

AMTD
3, 4497–4530, 2010

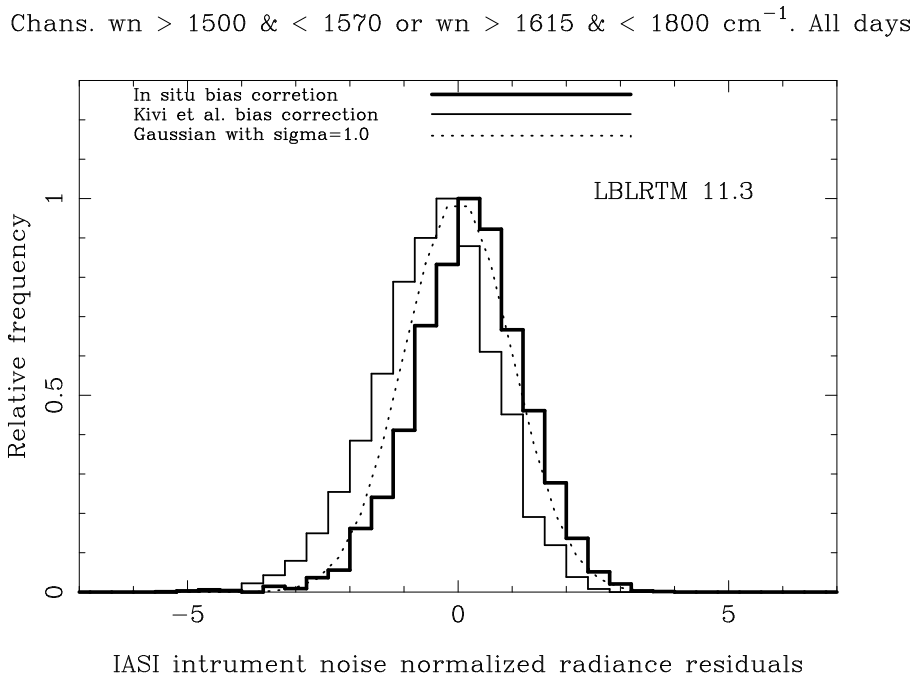

Fig. 10. Histogram of the residual radiances, IASI observed minus calculated with LBLRTM 11.3 RTM and two time interpolated profiles, for all clear days (4) in the spectral range, $1500\,\mathrm{cm}^{-1} \le \nu \le 1570\,\mathrm{cm}^{-1}$ and $1615\,\mathrm{cm}^{-1} \le \nu \le 1800\,\mathrm{cm}^{-1}$. One interpolated profile has been derived from the CFH sonde launched 1 h before IASI overpass and the "in situ" bias corrected RS92 sonde launched 5 min before satellite overpass (thick solid line). The other interpolated profile has been derived from the CFH sonde launched 1 h before IASI overpass and the Kivi et al. bias corrected RS92 sonde launched 5 min before satellite overpass (thin solid line). For reference, a Gaussian curve with a σ of 1.0 is shown (dotted line).

AMTD
3, 4497–4530, 2010

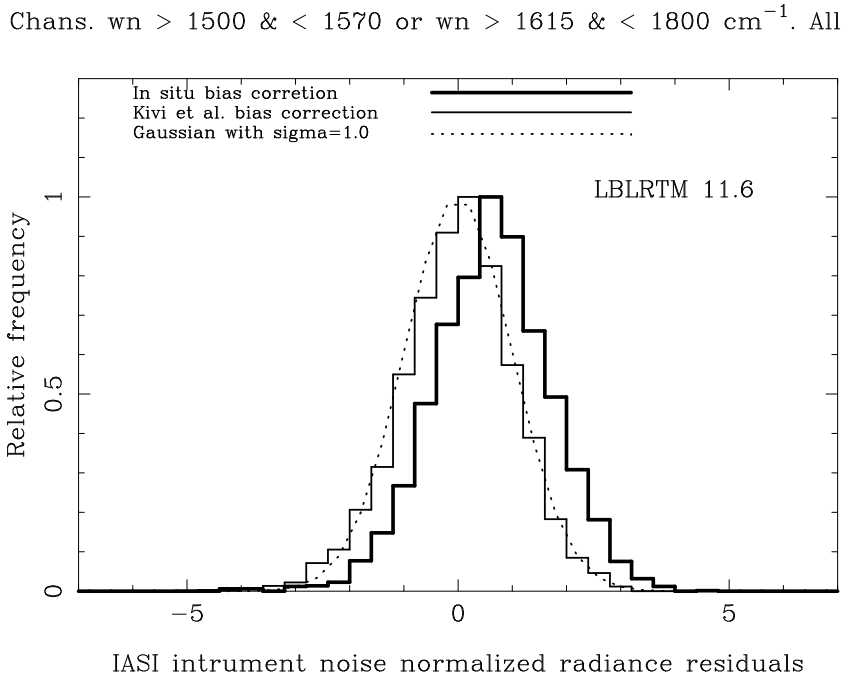

Fig. 11. Histogram of the residual radiances, IASI observed minus calculated with LBLRTM 11.6 RTM and two time interpolated profiles, for all clear days (4) in the spectral range, 1500 $cm^{-1} \leq wn \leq 1570\,cm^{-1}$ and 1615 $cm^{-1} \leq wn \leq 1800\,cm^{-1}$. One interpolated profile has been derived from the CFH sonde launched 1 h before IASI overpass and the "in situ" bias corrected RS92 sonde launched 5 min before satellite overpass (thick solid line). The other interpolated profile has been derived from the CFH sonde launched 1 h before IASI overpass and the Kivi et al. bias corrected RS92 sonde launched 5 min before satellite overpass (thin solid line). For reference, a Gaussian curve with a σ of 1.0 is shown (dotted line).

AMTD
3, 4497–4530, 2010

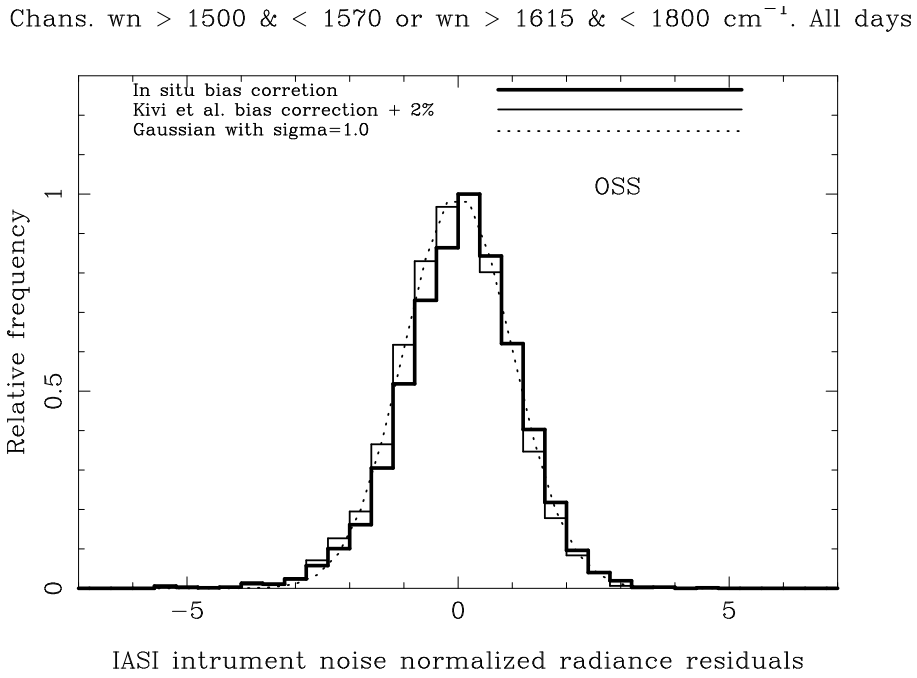

Fig. 12. Histogram of the residual radiances, IASI observed minus calculated with OSS RTM and two time interpolated profiles, for all clear days (4) in the spectral range, 1500 $cm^{-1} \leq$ wn $\leq$ 1570 cm^{-1} and 1615 $cm^{-1} \leq$ wn $\leq$ 1800 cm^{-1}. One interpolated profile has been derived from the CFH sonde launched 1 h before IASI overpass and the "in situ" bias corrected RS92 sonde launched 5 min before satellite overpass (thick solid line). The other interpolated profile has been derived from the CFH sonde launched 1 h before IASI overpass and the Kivi et al. +2% bias corrected RS92 sonde launched 5 min before satellite overpass (thin solid line). For reference, a Gaussian curve with a σ of 1.0 is shown (dotted line).

AMTD
3, 4497–4530, 2010

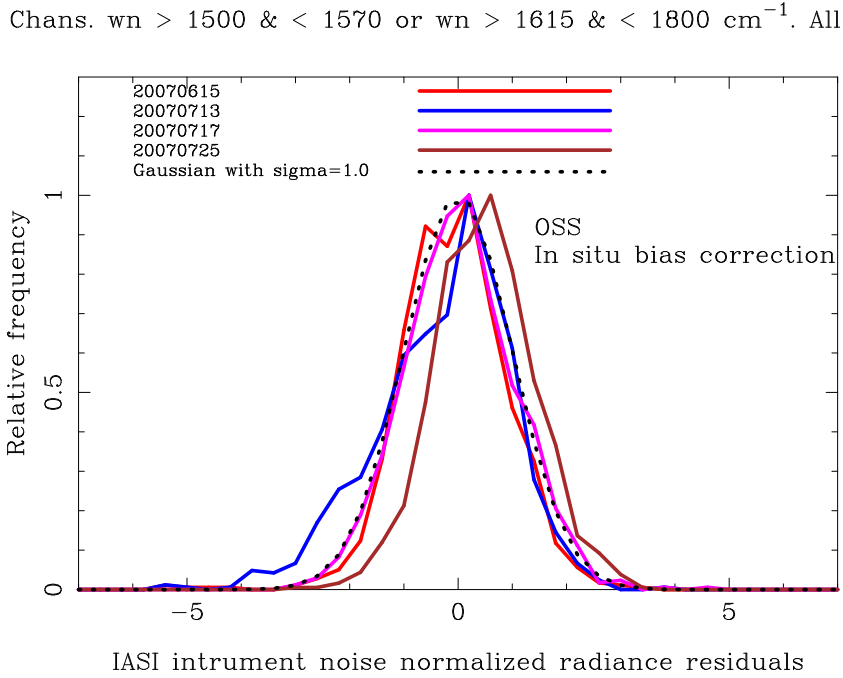

Fig. 13. Histogram of the residual radiances, IASI observed minus calculated with OSS RTM and one time interpolated profiles, for all clear days (4) in the spectral range, 1500 cm^{-1} ≤ wn ≤ 1570 cm^{-1} and 1615 cm^{-1} ≤ wn ≤ 1800 cm^{-1}. The interpolated profile has been derived from the CFH sonde launched 1 h before IASI overpass and the "in situ" bias corrected RS92 sonde launched 5 min before satellite overpass. The results for each one of the different observing days are shown independently in this figure. A one sigma Gaussian is shown as a dotted line.

AMTD
3, 4497–4530, 2010

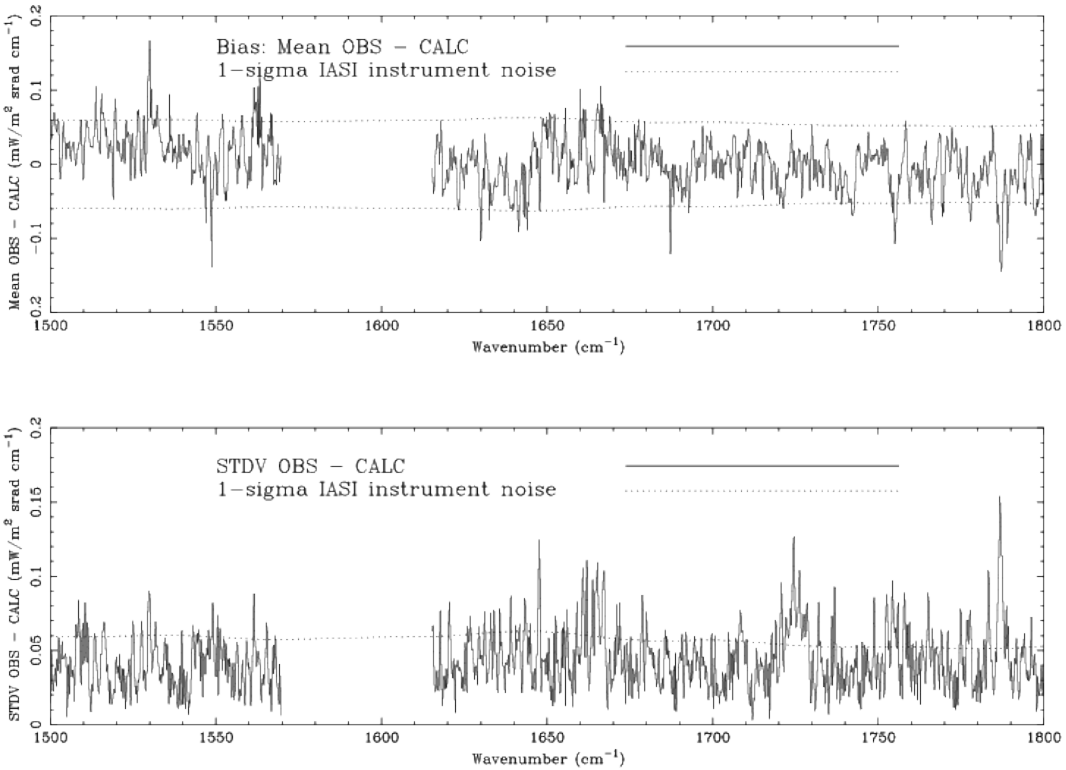

Fig. 14. Bias and standard deviation of IASI observed minus calculated radiances. The calculated radiances have been obtained using OSS and the "in situ" bias correction.

AMTD
3, 4497–4530, 2010